Supporting Information

Kinetics and Reaction Mechanism of Pd-Catalyzed Chlorobenzene Hydrogenolysis

Nikki Kragt, [1] Jalal Tavana, [2] Mohammed Al-Gharrawi,[2] M. Clayton Wheeler,[2] David Hibbitts,[1*] and Thomas J. Schwartz[2]*

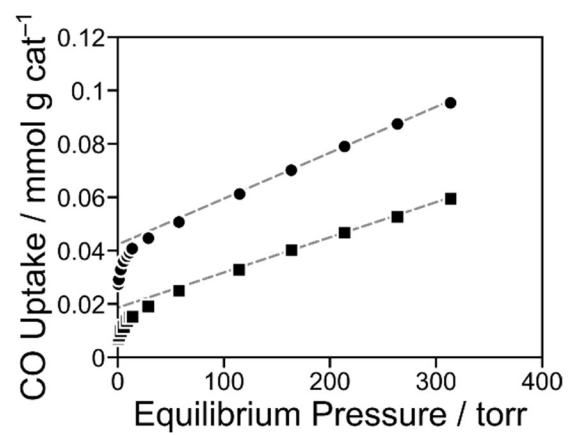[1]*Department of Chemical Engineering, University of Florida, Gainesville, FL 32611, USA*

[2]*Department of Chemical and Biomedical Engineering, University of Maine, Orono, ME 04469, USA*

*corresponding authors, email: hibbitts@ufl.edu, and thomas.schwartz@maine.edu

Table of Contents

Section S1. Determining particle size from CO uptake

Figure S1. Measured CO uptake of 24 μmol g^{-1} at 308 K on 5 wt% Pd/C particles. Circles (●) correspond to the first adsorption isotherm and squares (■) correspond to the second adsorption isotherm.

Section S2. Evaluating mass transfer limitations

TOFs as a function of stirring speed were measured to identify a regime in which external mass transfer limitations were not present. Increasing stirring speed decreases the boundary layer thickness between the catalyst surface and the bulk concentration. In Figure S2, we identify the point at which the boundary layer becomes thin enough that any potential concentration gradients are negligible, which identifies a regime where external mass transfer limitations are also negligible.
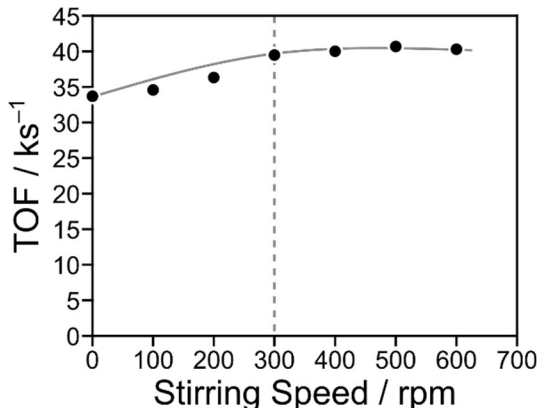
Figure S2. Hydrogenolysis TOFs on 14 nm 5% Pd/C particles at 353 K, 101 kPa H_2, 0.2 kPa PhCl, and 50% PhCl conversion.

Internal mass transfer limitations were evaluated by calculating the Weisz-Prater number and corresponding effectiveness factor for the regime identified (stirring speeds greater than 300 rpm). The Weisz-Prater number[1] is calculated as follows:

$$N_{\text{W-P}} = \frac{\Re R_P^2}{C_s D_{eff}}$$
(S1)

where $\Re$ is the observed rate, R_p is the radius of the catalyst particle, D_{eff} is effective diffusivity, and C_s is the reactant concentration at the particle surface. The steady-state effectiveness factor[2] (η; Eq. S2) is calculated from the resulting Weisz-Prater number.

$$\eta = 3 \left[\frac{1}{tanh\left(\sqrt{\frac{N_{\text{W-P}}}{\eta}}\right)} - \frac{1}{\sqrt{\frac{N_{\text{W-P}}}{\eta}}} \right]$$
(S2)

The Weisz-Prater criterion ($N_{\text{W-P}} = 0.047 \leq 1$) and corresponding effectiveness factor ($\eta = 0.98$) calculated for stirring speeds above 300 rpm, indicating that there are no meaningful concentration gradients within the catalyst pellets and negligible internal mass transfer limitations for this reaction.

Section S3. Measured reaction orders and corresponding uncertainties

Table S1. Measured reaction orders and corresponding uncertainties of kinetically relevant species at 313 K, 323 K, 343 K, and 353 K.

Species	Measured Reaction Orders			
	313 K	323 K	343 K	353 K
PhCl	−0.3±0.3	0.5±0.2	0.2±0.6	0.8±0.2
H_2	0.3±0.2	0.5±0.9	0.4±0.3	0.6±0.1
HCl	–	–	–	−0.9±2.4

Section S4. Kinetic isotope effect

The bond dissociation energies of breaking a C–H bond versus a C–D bond are different since D is a heavier atom; therefore, reactions involving breaking a C–D bond should occur at lower reaction rates than those breaking a C–H bond if such bond activations are kinetically relevant. Since reaction rates in the presence of H_2 and D_2 were not meaningfully different, we conclude that C–H bond activations prior to the rate-determining step are not kinetically relevant.
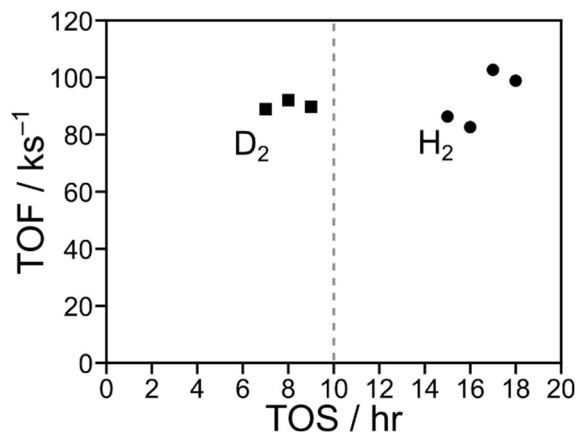
Figure S3. Hydrogenolysis TOFs on 5% Pd/C at 353 K and 50% PhCl conversion with deuterium (■), followed by hydrogen (●) as a reactant (0.7 kPa PhCl, 99.6 kPa H_2 or D_2, WHSV = 2.44 hr^{-1}).

Section S5. Single-site reaction mechanism and rate equations

Scheme S1 shows the direct application of Sinfelt's hydrogenolysis mechanism to PhCl hydrogenolysis. In this mechanism, PhCl adsorbs to a single surface site, which is followed by rate-determining C–Cl bond activation, with the resulting Cl* occupying an adjacent surface site. The Ph* and Cl* are removed by quasi-equilibrated hydrogenation with H* obtained by quasi-equilibrated hydrogen dissociation. Langmuir-Hinshelwood-Hougen-Watson analysis of this mechanism (*i.e.*, assuming PhCl*, Ph*, H*, and Cl* all compete equally for surface sites) leads to a rate equation with a squared denominator (Equation S3). Under conditions where Cl* can be assumed to be the MASI, Equation S3 simplifies to Equation S4 with apparent H_2 and HCl reaction orders of 1 and –2, respectively, which is inconsistent with our observations. Similarly, if PhCl* is the MASI (to explain the near-zero reaction order with respect to PhCl at 313 K), Equation S3 simplifies to Equation S5, characterized by apparent reaction orders of zero for H_2 and HCl and –1 for PhCl. While it could be argued that the PhCl reaction order would approach –1 if the temperature were further decreased, the reaction order with respect to H_2 is nearly invariant with changing temperature and a mechanism where PhCl*, Cl*, and H* all compete for sites cannot explain our observed reaction orders (or those given previously in the literature[3–5]). We also note that Equation S3 would govern the rate under conditions where PhCl* and Cl* compete for surface sites, which also does not match our observed reaction orders.

$$H_2\ (g) + 2^* \overset{}{\underset{K_1}{\rightleftharpoons}} 2H^* \qquad\qquad 1.1$$

$$HCl\ (g) + 2^* \overset{}{\underset{K_2}{\rightleftharpoons}} H^* + Cl^* \qquad\qquad 1.2$$

$$C_6H_5Cl\ (g) + {^*} \overset{}{\underset{K_3}{\rightleftharpoons}} C_6H_5Cl^* \qquad\qquad 1.3$$

$$C_6H_5Cl^* + {^*} \overset{}{\underset{k_4}{\longrightarrow}} C_6H_5^* + Cl^* \qquad\qquad 1.4$$

$$C_6H_5^* + H \overset{}{\underset{K_5}{\rightleftharpoons}} C_6H_6^* + {^*} \qquad\qquad 1.5$$

$$C_6H_6\ (g) + {^*} \overset{}{\underset{K_6}{\rightleftharpoons}} C_6H_6^* \qquad\qquad 1.6$$
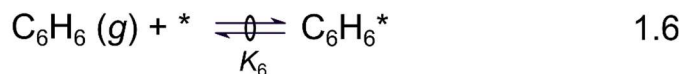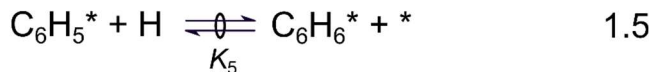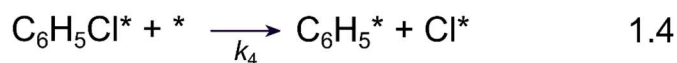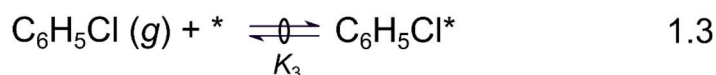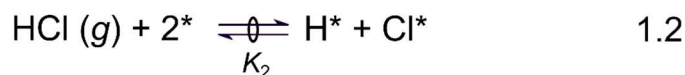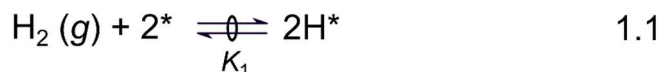
Scheme S1. Potential one-site mechanism following Sinfelt's mechanism for C-Cl hydrogenolysis[6] in methylamine (* denotes a vacant surface site).
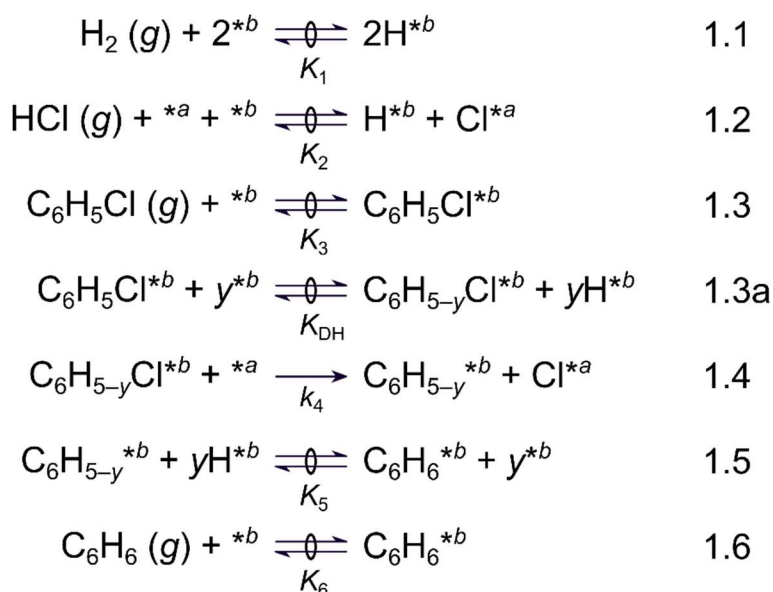
$$\frac{r}{[L]} = \frac{k_4 K_3 P_{PhCl}}{\left(1 + \sqrt{K_1 P_{H_2}} + K_3 P_{PhCl} + \frac{K_2 P_{HCl}}{\sqrt{K_1 P_{H_2}}}\right)^2} \qquad\qquad (S3)$$

$$\frac{r}{[L]} = \frac{k_4 K_3 P_{PhCl}}{\left(\frac{K_2 P_{HCl}}{\sqrt{K_1 P_{H_2}}}\right)^2} \qquad\qquad (S4)$$

$$\frac{r}{[L]} = \frac{k_4 K_3 P_{PhCl}}{(K_3 P_{PhCl})^2} \qquad\qquad (S5)$$

Section S6. Generalized reaction mechanism accounting for possible phenyl dehydrogenation

Scheme S2 differs from Scheme 1 in the main text by adding Step 1.3a, which represents possibly hydrogen removal from the phenyl ring prior to C–Cl bond activation. This in turn potentially alters the hydrogenation of the reactive intermediate and product phenyl in Steps 1.4 and 1.5. The hydrogen dependence of Step 1.5 is arbitrarily altered by y, or the number of hydrogens removed from the phenyl ring (Step 1.3a) and must then be added back to the phenyl ring (Step 1.5) prior to desorption of benzene (Step 1.6), but as Step 1.5 comes after the rate-determining step (Step 1.4), this change leaves the rate law virtually unaltered.

$$H_2\ (g) + 2*^b \underset{K_1}{\rightleftharpoons} 2H*^b \qquad\qquad 1.1$$

$$HCl\ (g) + *^a + *^b \underset{K_2}{\rightleftharpoons} H*^b + Cl*^a \qquad\qquad 1.2$$

$$C_6H_5Cl\ (g) + *^b \underset{K_3}{\rightleftharpoons} C_6H_5Cl*^b \qquad\qquad 1.3$$

$$C_6H_5Cl*^b + y*^b \underset{K_{DH}}{\rightleftharpoons} C_6H_{5-y}Cl*^b + yH*^b \qquad\qquad 1.3a$$

$$C_6H_{5-y}Cl*^b + *^a \xrightarrow{k_4} C_6H_{5-y}*^b + Cl*^a \qquad\qquad 1.4$$

$$C_6H_{5-y}*^b + yH*^b \underset{K_5}{\rightleftharpoons} C_6H_6*^b + y*^b \qquad\qquad 1.5$$

$$C_6H_6\ (g) + *^b \underset{K_6}{\rightleftharpoons} C_6H_6*^b \qquad\qquad 1.6$$

Scheme S2. Proposed two-site mechanism including the possibility of dehydrogenation of the phenyl ring prior to bond cleavage.

Section S7. Additional computational details

VASP provides the electronic energy (E_0) of an optimized structure at 0 K. Frequency calculations were used to calculate vibrational frequencies (v_i) that were then used to determine the zero-point vibrational energy (ZPVE) and vibrational contributions to enthalpy and free energy (H_{vib}, G_{vib}). Zero-point vibrational energy (ZPVE) and the vibrational, rotational, and translational contributions of enthalpy (H_{vib}, H_{rot}, H_{trans}) and free energy (G_{vib}, G_{rot}, G_{trans}) were determined from statistical mechanics.[7] These terms were added together to estimate temperature-corrected enthalpies (H) and free energies (G) at 353 K.

$$H = E_0 + \text{ZPVE} + H_{vib} + H_{trans} + H_{rot} \tag{S6}$$

$$G = E_0 + \text{ZPVE} + G_{vib} + G_{trans} + G_{rot} \tag{S7}$$

$$\text{ZPVE} = \sum_i \frac{1}{2} h v_i \tag{S8}$$

$$H_{vib} = \sum_i \frac{h v_i e^{\frac{-h v_i}{kT}}}{1 - e^{\frac{-h v_i}{kT}}} \tag{S9}$$

$$H_{trans} = \frac{5}{2} kT \tag{S10}$$

$$H_{rot,linear} = kT \tag{S11}$$

$$H_{rot,nonlinear} = \frac{3}{2} kT \tag{S12}$$

$$G_{vib} = \sum_i -kT \ln\left(\frac{1}{1 - e^{\frac{-h v_i}{kT}}}\right) \tag{S13}$$

$$G_{trans} = -kT \ln\left[\left(\frac{2\pi M}{h^2}\right)^{\frac{3}{2}} V\right] \tag{S14}$$

$$G_{rot} = -kT \ln\left[\frac{\pi^{\frac{1}{2}}}{\sigma}\left(\frac{T^3}{\theta_x \theta_y \theta_z}\right)^{\frac{1}{2}}\right] \tag{S15}$$

$$\theta_i = \frac{h^2}{8\pi^2 k I_i} \tag{S16}$$

In equations S6–S16, h is Planck's constant, k is the Boltzmann constant, T is temperature, M is the mass of the molecule, V is the volume of the unit cell, σ is the symmetry number of the molecule, and I_i is the moment of intertia about axis i. For gas molecules, all vibrational, translational, and rotational contributions were computed. For calculations of adsorbed species on a periodic metal surface, the translational and rotational degrees of freedom are assumed frustrated and treated as vibrations.

Section S8. Electronic adsorption energies of H* and PhCl* on Cl*-covered surfaces including dispersion

Dispersive interactions can contribute significantly to adsorption free energies and do so in an asymmetric way that correlates with molecule size. Tables S2 and S3 show adsorption energies for H* and PhCl* with and without dispersive interactions. Note that values in Table S2 are referenced to ½H$_2$ in the gas. DFT-calculated adsorption energies of H* on Cl*-covered surfaces including dispersion are relatively constant near -37 kJ mol^{-1} for Cl* coverages from 0–0.1875 ML (3 Cl* on a 4×4 Pd (111) surface), then they increase to -20 kJ mol^{-1} at 0.25 ML. While there is a co-adsorbate repulsion between H* and Cl* at coverages ≥ 0.25 ML, we don't expect the repulsion is enough to prevent adsorption of H* in those interstitial regions based on H* adsorption energies on Cl*-free surfaces. Adsorption energies for PhCl* with dispersion are ~130 kJ mol^{-1} more exothermic than those without and can be taken to estimate adsorption free energies (with dispersive interactions) that are -45 or -35 kJ mol^{-1}, depending on Cl* coverage at 353 K. At lower temperatures (e.g. 313 K) the entropy losses in PhCl* upon adsorption will be less impactful on the adsorption free energy, and thus the values will be more negative.

Table S2. Electronic adsorption energies of H* on Cl*-covered surfaces without (RPBE) and with (RPBE-D3) dispersive interactions.

| Cl* Coverage ML	RPBE kJ mol^{-1}	RPBE-D3 kJ mol^{-1}
0	-38	-45
0.0625	-38	-45
0.1250	-37	-44
0.1875	-36	-42
0.2500	-20	-29
0.3125	-18	-27

Table S3. Electronic adsorption energies of PhCl* without (RPBE) and with (RPBE-D3) dispersive interactions.

Cl* Coverage ML	RPBE kJ mol^{-1}	RPBE-D3 kJ mol^{-1}
0	-2	-131
0.0625	2	-129
0.125	7	-127
0.1875	30	-109
0.25	48	-97
0.3125	97	-50

Section S9. Free energy and enthalpy reaction barriers on bare Pd(111) model
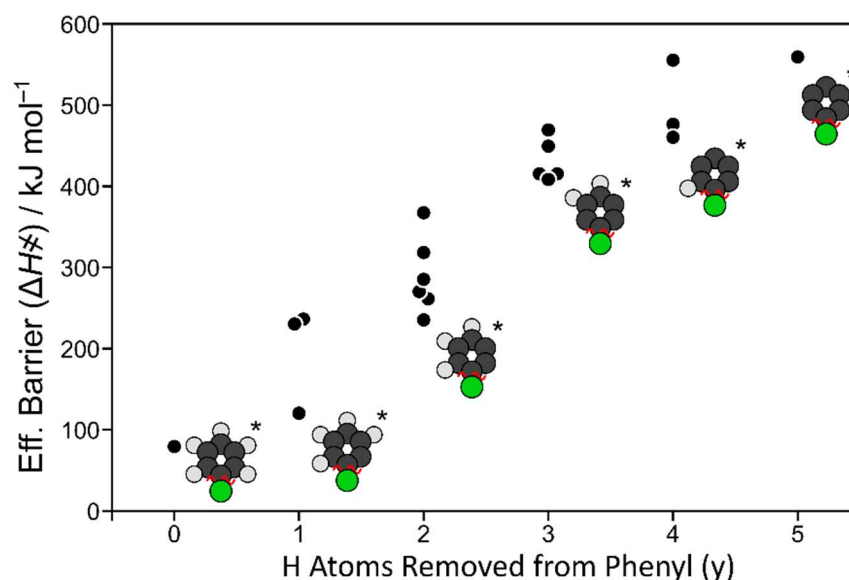

Figure S4. Enthalpy barriers ($\Delta H\ddagger$; Eq. 7) for C–Cl bond activation in PhCl-derived adsorbates on a bare 4×4 Pd(111) surface model (353 K, 1 bar H_2), where isomers corresponding to the lowest activation barrier at each saturation level are shown.

Table S4. Tabulated data for enthalpy and free energy barriers for C–Cl in PhCl-derived adsorbates on a bare 4×4 Pd(111) surface model (353 K, 1 bar H_2).

Structure	y	$\Delta H\ddagger$ / kJ mol^{-1}	$\Delta G\ddagger$ / kJ mol^{-1}
-Cl-CHCHCHCHCH-	0	78	146
-C-Cl-CCHCHCHCH-	1	119	165
-C-Cl-CHCCHCHCH-	1	235	280
-C-Cl-CHCHCCHCH-	1	229	284
-C-Cl-CHCHCHCC-	2	234	264
-C-Cl-CHCHCCCH-	2	260	290
-C-Cl-CCHCHCHC-	2	269	295
-C-Cl-CHCHCCHC-	2	317	344
-C-Cl-CHCCHCCH-	2	366	390
-C-Cl-CHCCHCHC-	2	284	315
-C-Cl-CHCHCCC-	3	407	410
-C-Cl-CHCCCCH-	3	440	440
-C-Cl-CHCCHCC-	3	441	444
-C-Cl-CHCCCHC-	3	461	463
-C-Cl-CCHCHCC-	3	400	405
-C-Cl-CCHCCHC-	3	407	414
-C-Cl-CHCCCC-	4	459	443
-C-Cl-CCHCCC-	4	475	459
-C-Cl-CCCHCC-	4	554	536
-C-Cl-CCCCC-	5	558	519

Section S10. Differential binding free energies and enthalpies for Cl* coverage on Pd(111)
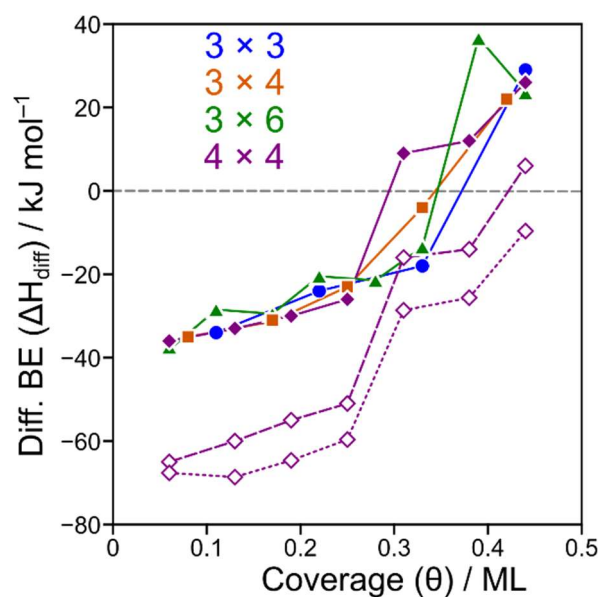
**Figure S5.** Differential binding enthalpies (ΔH_{diff}) for incrementally adding Cl* to lowest energy configurations on 3 × 3 (blue ●), 3 × 4 (orange ■), 3 × 6 (green ▲), and 4 × 4 (purple ◆) Pd(111) surface models (353 K). Additionally, calculations on the 4 × 4 surface model were also performed using the PBE functional (hollow purple ◆; dashed line) and RPBE-D3 functional (hollow purple ◆; dotted line).

Table S5. Tabulated data for differential enthalpies and free energies for incrementally adding Cl*
to the lowest energy configurations on Pd(111) surface models (353 K).

Pd(111) Surface Size	θ / ML	ΔH_{diff} / kJ mol^{-1}	ΔG_{diff} / kJ mol^{-1}
3 × 3	1/9	−34	−4
	2/9	−24	3
	1/3	−18	9
	4/9	29	53
3 × 4	1/12	−35	−7
	1/6	−31	−2
	1/4	−23	4
	1/3	−4	20
	5/12	22	55
3 × 6	1/18	−38	−9
	1/9	−29	0
	1/6	−30	−1
	2/9	−21	7
	5/18	−22	6
	1/3	−14	13
	7/18	−28	65
	4/9	85	46
4 × 4	1/16	−36	−8
	1/8	−33	−5
	3/16	−30	−2
	1/4	−26	1
	5/16	9	36
	3/8	12	38
	7/16	26	55
4 × 4 (PBE)	1/16	−65	−35
	1/8	−60	−30
	3/16	−55	−26
	1/4	−51	−22
	5/16	−16	18
	3/8	−14	6
	7/16	6	42
4 × 4 (RPBE-D3)	1/16	−68	−41
	1/8	−69	−40
	3/16	−65	−37
	1/4	−60	−33
	5/16	−29	−2
	3/8	−26	0
	7/16	−10	19

Section S11. Free energy and enthalpy reaction barriers on Cl*-covered Pd(111) model
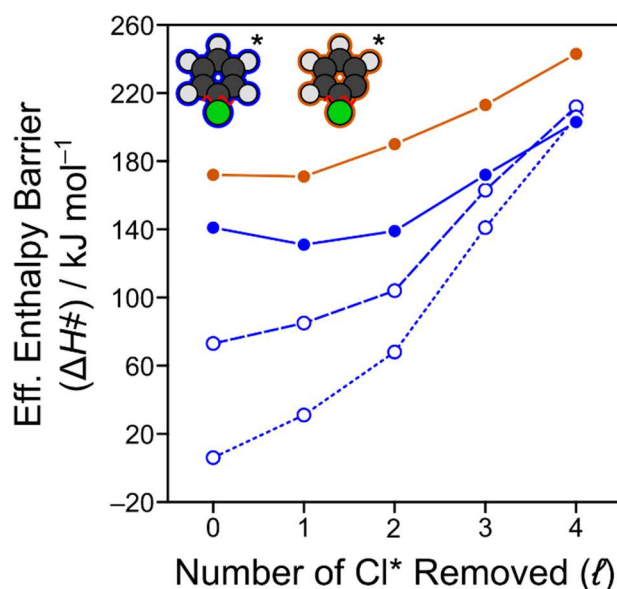
Figure S6. Enthalpy barriers ($\Delta H^{\ddagger}$; Eq. 7) of C–Cl bond activation for PhCl* (blue) and *ortho*-C_6H_4Cl* (orange) as a function of Cl* removed from the surface before bond activation on a 4×4 Pd(111) surface model with 4Cl* (353 K, 1 bar H_2). Solid points were calculated with the RPBE functional, whereas hollow points were calculated with PBE (dashed line) and RPBE-D3 (dotted line).

Table S6. Tabulated data for enthalpy and free energy barriers of C–Cl bond activation for PhCl* and *ortho*-C_6H_4Cl* as a function of Cl* removed from the surface before bond activation on a 4×4 Pd(111) surface model with 4Cl* (353 K, 1 bar H_2).

Pd(111) Surface Size	ℓ	$\Delta H^{\ddagger}$ / kJ mol^{-1}	$\Delta G^{\ddagger}$ / kJ mol^{-1}
PhCl*	4	203	161
	3	172	154
	2	139	148
	1	131	168
	0	141	203
ortho-C_6H_4Cl*	4	243	179
	3	213	178
	2	190	182
	1	171	190
	0	172	219
PhCl* (PBE)	4	212	164
	3	163	142
	2	104	112
	1	85	125
	0	73	136
PhCl* (RPBE-D3)	4	206	163
	3	141	123
	2	68	77
	1	31	69
	0	6	68

Section S12. References

[1]   P.B. Weisz, C.D. Prater, Interpretation of measurements in experimental catalysis, in: Elsevier, 1954: pp. 143–196. https://doi.org/10.1016/S0360-0564(08)60390-9.

[2]   O. Levenspiel, Chemical Reaction Engineering, 3rd Edition, 3rd ed., Wiley, New York, 1998.

[3]   C.D. Thompson, R.M. Rioux, N. Chen, F.H. Ribeiro, Turnover rate, reaction order, and elementary steps for the hydrodechlorination of chlorofluorocarbon compounds on palladium catalysts, J. Phys. Chem. B. 104 (2000) 3067–3077. https://doi.org/10.1021/jp992888n.

[4]   B. Coq, Conversion of chlorobenzene over palladium and rhodium catalysts of widely varying dispersion, J. Catal. 101 (1986) 434–445. https://doi.org/10.1016/0021-9517(86)90271-X.

[5]   K. Konuma, N. Kameda, Effect of substituents on the hydrodechlorination reactivity of para-substituted chlorobenzenes, J. Mol. Catal. A: Chem. 178 (2002) 239–251. https://doi.org/10.1016/S1381-1169(01)00337-5.

[6]   J.H. Sinfelt, Catalytic hydrogenolysis on metals, Catal. Lett. 9 (1991) 159–171. https://doi.org/10.1007/BF00773174.

[7]   D.A. McQuarrie, Statistical mechanics, University Science Books, Sausalito, Calif, 2000.